EULER ANALYSIS OF AN ELLIPTIC MISSILE BODY
AT ANGLES OF ATTACK

James R. Sirbaugh
Air Force Wright Aeronautical Laboratories
Wright-Patterson Air Force Base, Ohio

SUMMARY

The Euler code FL057 has been applied to a blunt nose smooth surface missile body shape. A range of angle of attacks was analyzed at Mach numbers of 0.55 and 2.0. A Mach number sweep from 0.55 to 2.0 was run for 12 degrees angle of attack. Experimental force and moment data were compared to Euler results at all Mach numbers and surface pressure data were compared at Mach 2.0. The Euler code agreed with the experimental data over the linear portion of the Mach 0.55 data and over the entire angle-of-attack range at Mach 2.0.

INTRODUCTION

The capability to predict aerodynamic characteristics of smooth surfaced missile bodies is required by weapons designers. Missile body prediction techniques need to be able to analyze subsonic, transonic, supersonic flows, subsonic pockets in supersonic flow and vortex flow. At present there is no available numerical method to analyze these flow regimes within reasonable time and cost limits. The Navier-Stokes equations are the most logical choice to perform the analysis, but at present, computers and algorithms are too slow to make the analysis practical. The Euler equations have been successfully applied to the Mach range in question, but viscous effects are not accounted for and therefore vortex flow prediction may be inaccurate. Other techniques are available which have a more limited range of application, such as full-potential, parabolized Navier-Stokes and free vortex sheet theory.

This paper presents the results of applying the Euler code FL057 to an elliptical missile body for a Mach number range of 0.55 to 2.0. The motivation behind the work was to determine if FL057 could be used to predict the aerodynamic characteristics of simple missile shapes at low supersonic speeds, where subsonic pockets exist at blunt noses and vortex flow exists at moderate angles of attack. At present only hybrid methods are used to analyze these flow conditions in a reasonable time limit. In addition to investigating the use of FL057 for low supersonic Mach numbers, subsonic and transonic Mach numbers were also considered.

SYMBOLS

A	Missile body semi-major axis at a given body X-station
AL	Angle of attack
A_{max}	Missile body base semi-major axis
B	Missile body semi-minor axis at a given body X-station
B_{max}	Missile body base semi-minor axis
C_A	Axial force coefficient
C_M	Pitching moment coefficient
C_N	Normal force coefficient
C_p	Coefficient of pressure
I, J, K	Grid coordinates
L	Missile body length
M_∞	Freestream Mach number
X	Missile body station measured relative to nose
3-D	Three dimensional

CONFIGURATION

The missile body is a simple shape built and tested for the purpose of developing and validating aerodynamic prediction methods. The missile body was one of three built with elliptical cross sections along the entire length of the model. The missile body used in this study had a 2.5 to 1.0 major to minor axis ratio (Figure 1). The two other missile bodies built had 2.0 to 1.0 and a 3.0 to 1.0 cross-section ratios. The semi-major axis varied along the body by the square root law

$$A = \frac{A_{max}}{L^{\frac{1}{2}}} X^{\frac{1}{2}}$$

and the semi-minor axis varied along the body by the square root law

$$B = \frac{B_{max}}{L^{\frac{1}{2}}} X^{\frac{1}{2}}$$

A_{max} and B_{max} were the base semi-major and semi-minor axes and L was the missile body length. These missile bodies were tested in four stages. Stage one produced surface pressure data from eleven rows of spanwise pressure taps at Mach numbers from 1.5 to 5.0. During stage two, force and moments were taken for Mach numbers of 1.76 to 5.0. Stage three was a force and moment test for Mach numbers of 0.4 to 1.3. Stage four data were not available at the time of this analysis and were the Mach numbers 0.4 to 1.3 pressure tests. All testing was done at Arnold Engineering Development Center. References 1 and 2 contain detailed information of the test results.

EULER GRID AND FLOW SOLVER

The grid used for the Euler calculations was originally developed for predicting flow fields about delta wings and was modified for use on the test missile body shape. The grid topology is intended to provide adequate grid resolution at the missile nose while positioning the grid singularity on the plane of symmetry and out of regions of high flow gradients (Figure 2). The topology can best be thought of as a sheared O-H grid. Indicated in Figure 3 are the coordinate directions on the missile surface and a cut through the 3-D grid. The O portion of the O-H grid is formed by the I indexing grid lines that start on the lower plane of symmetry aft of the grid singularity and follow a path along the missile surface, around the leading edge and back to the upper plane of symmetry. The J indexing lines start at the missile surface and proceed outward to the far field. The K indexing lines start on the plane of symmetry forward of the grid singularity and follow paths along the missile going aft. Figure 4 is the downstream exit grid or maximum K grid layer. The base of the missile was extended downstream with solid surface boundary conditions being applied to the extension's outer surface. This extension does not resemble the wind tunnel model, but was required to perform the computations. The grid had 49 grid points in the I or wrap-around direction and 44 points in the K direction on the missle surface. There were 25 J layers of grid points extending outward from the surface to the far-field boundary.

The flow solver used was FLO57 without any special treatment for vortex flows (Reference 3). FLO57 has been applied previously to round and sharp leading-edge delta wing vortex flow problems for both subsonic and transonic Mach numbers. No attempt was made in generating the missile grid to align the 3-D grid with the bow shock shape. The bow shock is dependent on the configuration angle of attack (AL) and freestream Mach number. The Euler solution scheme uses centered difference approximation to the flux terms. Shock smearing will occur when the bow shock is unaligned with the grid, introducing an unknown amount of error in the solution. At the immediate nose of the configuration the shock should approximate the shape of the blunt nose and therefore align with the grid at moderate supersonic Mach numbers.

FORCE AND MOMENT RESULTS

C_N Versus Alpha, $M_\infty = 0.55$

FL057 predicted lower C_N's at Mach 0.55 (Figure 5) than were measured in the wind tunnel test in the nonlinear portion of the C_N versus the Alpha curve. At the low angle-of-attack range (0.0 - 6.0 degrees) the Euler and wind tunnel test results are in excellent agreement. It appears that the Euler method is not predicting vortex flow that is present in the wind tunnel data at the higher angles of attack.

C_A Versus Alpha, $M_\infty = 0.55$

The axial force coefficient was not measured directly in the wind tunnel test but was calculated by subtracting the measured base axial force from the balance measured total axial force. Two wind tunnel data points are plotted at each 2.0 and 4.0 degrees on Figure 6 corresponding to plus and minus angles of attack and indicate the degree of uncertainty of the wind tunnel axial force coefficients. The Euler results are inviscid and do not reflect skin friction axial force. To permit direct comparisons of the wind tunnel and Euler results the wind tunnel C_A's have been shifted to match the Euler results at 0.0 degrees angle of attack. This shifting of wind tunnel is only useful if the axial force due to skin friction is constant at all angles of attack for a given Mach number. The wind tunnel C_A at 0.0 degrees angle of attack is due only to skin friction. The predicted Euler results are in general agreement with the experimental data.

C_M Versus C_N, $M_\infty = 0.55$

The slopes of the C_M versus C_N curves (Figure 7) at $C_N = 0.0$ for the Euler and wind tunnel data are in excellent agreement. Above a C_N value of 0.7 the two curves are in disagreement indicating the vortex contribution to C_M is not present in the Euler results.

C_N Versus Alpha, $M_\infty = 2.0$

The predicted Euler C_N values (Figure 8) are in excellent agreement with the wind tunnel data below 6.0 degrees angle of attack. Above 6.0 degrees the curve slopes of the two sets of data are in excellent agreement but appeared to be shifted by approximately 0.5 degrees angle of attack. There are several possible sources of the Euler angle-of-attack shift, although it is not clear as to which factor is most important. The Euler results are inviscid and therefore are missing the physics of boundary layer separation in the vortex region. The angle-of-attack shift is a delay in vortex formation which may be attributed to missing viscous effects. Another possible source of the angle-of-attack shift

is the smearing of the bow shock due to misalignment of the low shock and grid. Since FL057 is inviscid and little if any vortex lift was apparent in the Mach 0.55 results (Figure 5), the assumption must be made that the Mach 2.0 vortex formation is due largely to entropy production through the bow shock. Any smearing of the bow shock can effect the amount of entropy produced by the bow shock and thus shift the C_N versus curve.

C_A Versus Alpha, M_∞ = 2.0

The wind tunnel test C_A's have been shifted to match the Euler C_A value at 0.0 degree of angle of attack (Figure 9). The predicted values and trends of the Euler C values are in general agreement with the experimental data. The uncertainty of the experimental C_A's was as great as 0.0056 at 4.0 degrees angle of attack.

C_M Versus C_N, M_∞ = 2.0

The Euler C_M versus C_N curve (Figure 10) is in good agreement with the wind tunnel data both in magnitude and in slope.

C_N Versus Mach, Alpha = 12.0°

The Euler predicted C_N values were shown to disagree with the experimental data at subsonic and transonic Mach numbers by a large amount. The agreement improved as the Mach increased from 1.3 to 2.0 as shown in Figure 11.

ΔC_N Versus Mach, Alpha = 12.0°

A ΔC_N parameter is plotted in Figure 12. The ΔC_N is the vortex-induced increment or nonlinear addition to the C_N due to the vortex. The wind tunnel test ($\partial C_N / d\alpha$) slope at zero angle of attack was multiplied by 12.0 degrees to compute a linear value of C_N at 12.0 degrees. The difference between the experimental value of C_N and computed linear C_N is ΔC_N. The same extrapolation was used to compute ΔC_N for the Euler results. Several interesting observations can be made by studying Figure 12. The experimental curve can be broken into two regions based on Mach number range. Region one is the subsonic and low supersonic Mach number range where the bow shock is weak. Region two starts about Mach 1.25 or 1.30, where the bow shock is strong enough to produce entropy. The two regions have different slopes and should be thought of as the viscous separation dominated region and bow shock entropy addition region.

The Euler results appear to have a more strongly Mach number dependent shape. At a purely subsonic Mach number of 0.55, ΔC_N is very low and only increases a small amount by going to Mach 0.8 in comparison to the experimental data. At Mach numbers from 1.3 to 1.75 the Euler curve is considerably steeper than the experimental data. Mach 1.3 is the point where entropy levels begin to be strongly influenced by shock strength. It appears that the Euler ΔC_N is

predominately a function of bow shock entropy production and not numerical or artificial viscosity. The Euler and experimental values of ΔC_N at Mach numbers of 1.75 and 2.0 appear in reasonable agreement as was previously shown in Figure 8.

C_M Versus Mach, Alpha = 12.0°

The Euler predicted value of C_M is relatively independent of Mach number. Only a slight decrease in C_M appears at transonic Mach numbers. The wind tunnel data indicated a strong dependency on Mach number in the Mach 0.8 to 1.1 range. Above Mach 1.3 the Euler and experimental values of C_M are in good agreement. A discrepancy in C_M between Euler and experiment appears at a Mach number of 2.0 in Figure 13, but is not as apparent in Figure 10.

SURFACE PRESSURE DATA

The Euler and wind tunnel C_p values are plotted against semi-span for four X-stations in Figures 14-25. The nose of the missile is X = 0.0 station and the missile base is X = 36.0 station. The computational grid points did not lie precisely on the required X-stations; therefore, all computational grid points within a prescribed distance to the required X-station were plotted. The method of selecting a computational grid was examined for accuracy and does not contribute any discrepancies that may be visible in the C_p comparison plots, Figures 14-25.

The 4.0 degree angle-of-attack results indicated an attached "potential like" flow over the entire length of the missile (Figures 14-17). The Euler results agree in shape with the wind tunnel data, but appear to be shifted in a more negative C_p direction than the wind tunnel results. At 8.0 degrees angle of attack the Euler results still indicate an attached "potential like" flow while the experimental data have signs of vortex separation starting at X-station 16.0 (Figures 18-21). The shift in C_p of the Euler results still appears and is roughly of the same magnitude. The C_p shift is constant even at 12.0 degrees angle of attack (Figures 22-25) on the lower surface. The reason for C_p shift is not obvious and may be due to not properly capturing the bow shock. A smeared bow shock can introduce angularity to the flow impinging on the missile body and create an apparent angle-of-attack shift. At 12.0 degrees angle of attack both the Euler and wind tunnel data indicate vortex separation (Figures 22-25). The wind tunnel data indicate a more forward separation point than does the Euler results. At X-stations 25.6 and 35.2 (Figures 24 and 25) the Euler and experimental C_p's indicate that the secondary vortex may have a significant effect on the strength and position of the primary vortex. The Euler results have a single vortex that has a larger peak pressure and is more outboard than the experimental data. The secondary vortex is also visible in the experimental data. The effect of a secondary vortex is to move the primary vortex inboard and thus reduce the peak pressure of the primary vortex.

VORTEX FLOW FIELD

Plotted in Figure 26 is the velocity flow field at the X-station 35.2 for Mach 2.0 and 12.0 degrees angle of attack. The vortex region can clearly be seen along with the high velocities occurring at the leading edge. To better visualize the flow region, a "constrained particle path" plot was made (Figure 27). At different locations in the X-station 35.2 vertical plane particles are released and allowed to trace paths as they are carried along by the cross flow velocities. The components of velocity aligned with the body axis are considered zero in this process, causing all "particles" to remain in the X-station vertical plane. The area of vortex flow is clearly visible. Figure 28 is a plot of local static pressure normalized by freestream and should provide information valuable to a designer.

CONCLUDING REMARKS

The accuracy of the FL057 Euler code is dependent on Mach number for the blunt nose smooth surface missile body used in this investigation. The formation and strength of the vortex appear dependent on the supersonic nose shock and not on surface viscous effects. The code is accurate and useful in the linear angle-of-attack range at both subsonic and supersonic Mach numbers. Sufficient entropy is produced by bow shocks at Mach numbers of 1.7 and above to confidently apply the code at higher angles of attacks for freestream Mach numbers above 1.7.

All Euler calculations presented in this paper were generated on the NASA Ames Cray XMP computer using approximately 0.9 million words in core and 1.0 million words out of core. All out-of-core memory resided on the 16 million word SSD using "buffer in" and "buffer out" statements to transfer data. A typical case required 500 iterations to converge from an initial guess of freestream conditions, which corresponds to approximately 600.0 seconds of CPU time and 10.0 seconds of IO time. Convergence criteria were an average residual of 1.0×10^{-5} plus C_N and C_A remaining constant for 20 iterations.

REFERENCES

1. Amidon, P.F., "Supersonic Aerodynamic Characteristics of Elliptical Cross Section Bodies," AIAA Paper No. 85-1607, 1985.

2. Sellers, M.E., "Static Stability Test of Three Elliptic Missile Body Configurations," Arnold Engineering Development Center, Telehoma, Tenn., AEDC-TSR-85-P8, May 1985.

3. Jameson, A., and Baker, T.J., "Multigrid Solution of the Euler Equations for Aircraft Configurations," AIAA Paper No. 84-0093, 1984.

2.5: 1.0 ELLIPTIC MISSILE BODY

TOP VIEW

SIDE VIEW
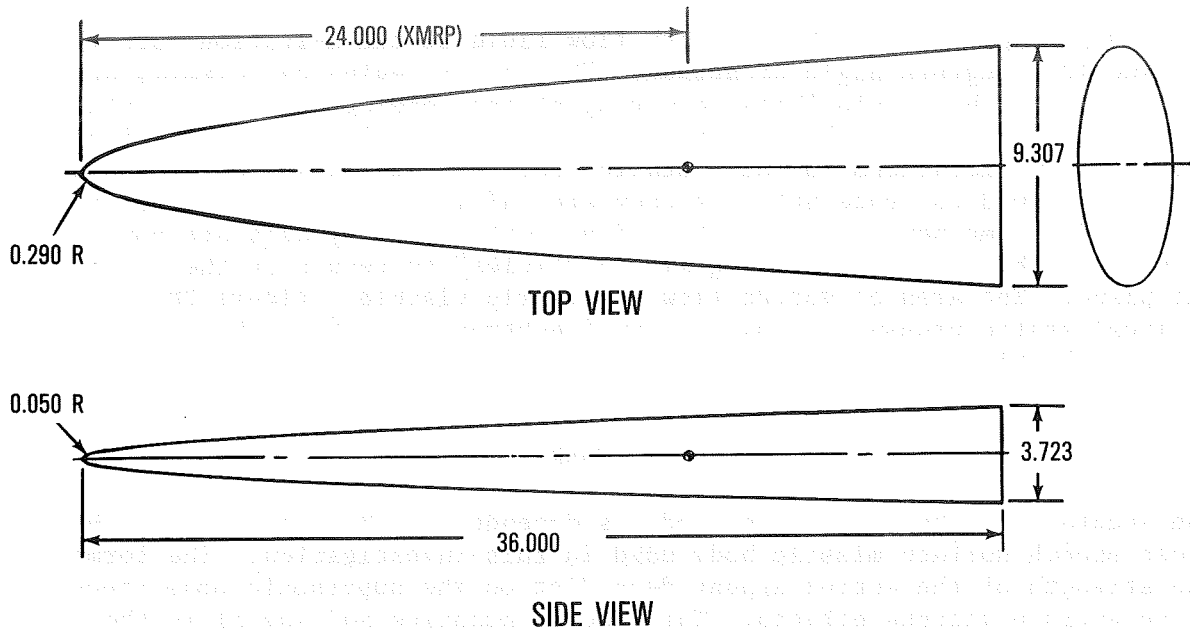
Figure 1.- Wind tunnel model (from ref. 2).
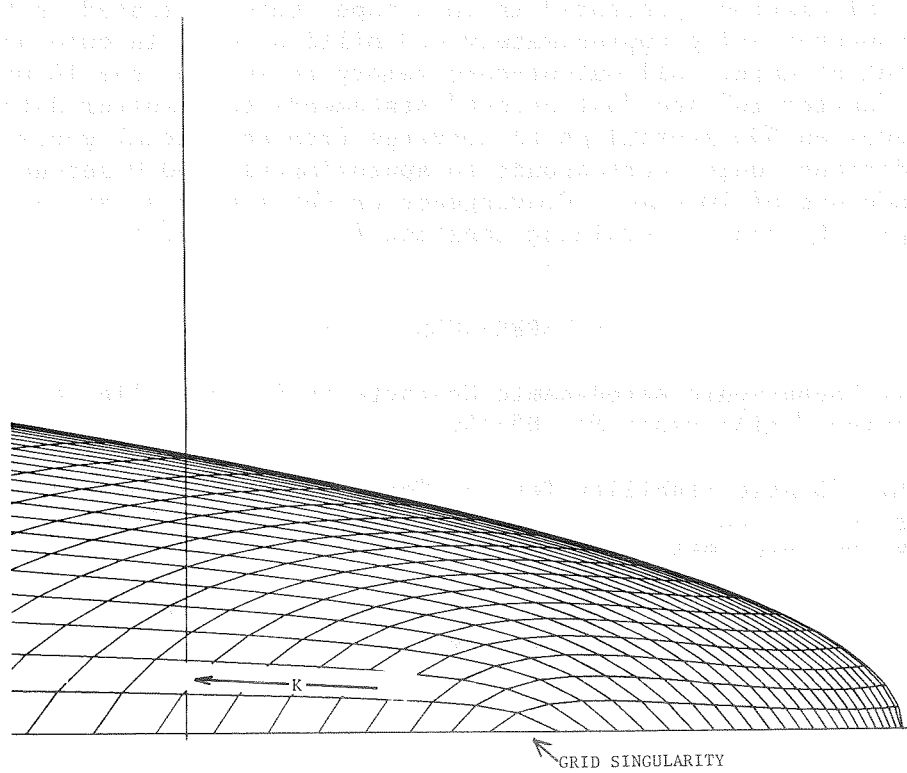
Figure 2.- Missile surface grid in nose region.

GRID SINGULARITY
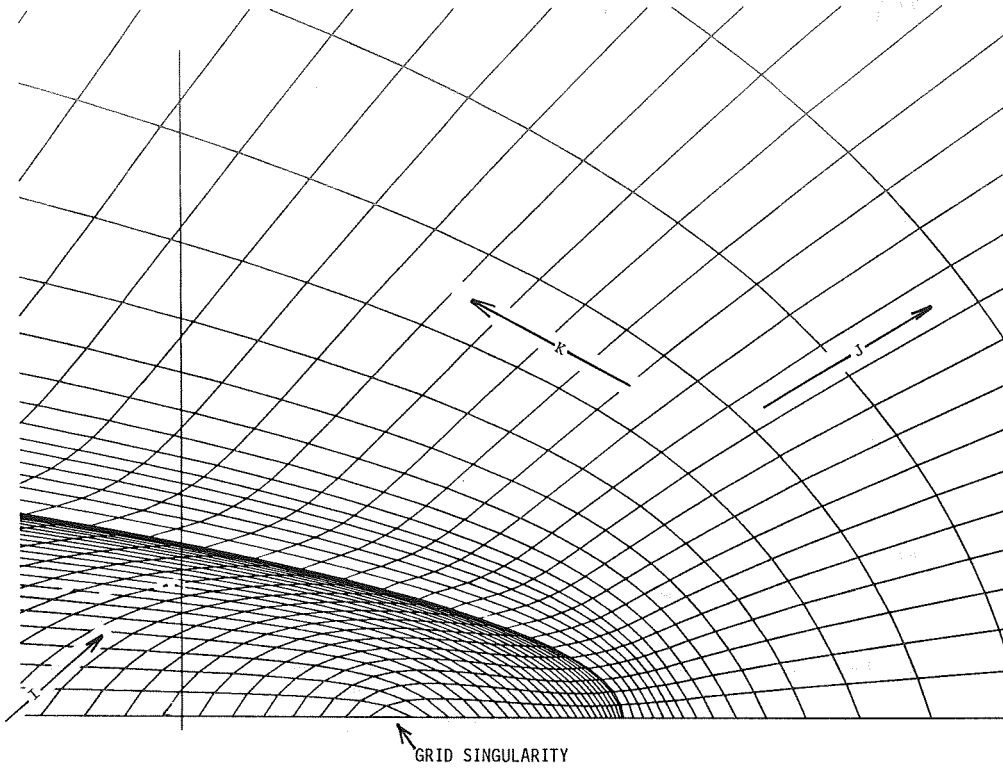
Figure 3.- Missile 3-D grid.
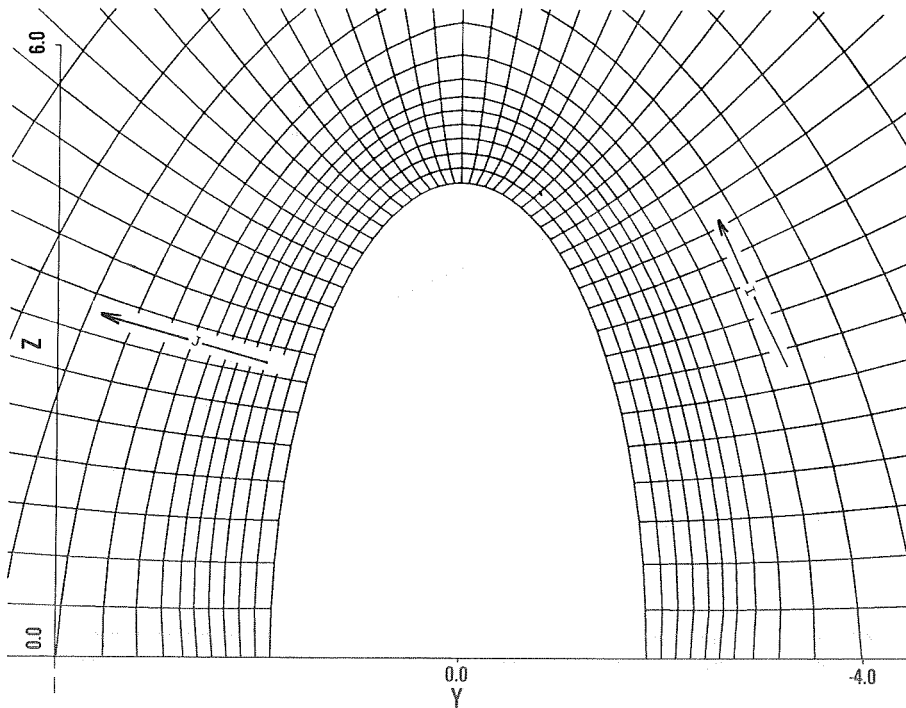
Figure 4.- Missile base grid.
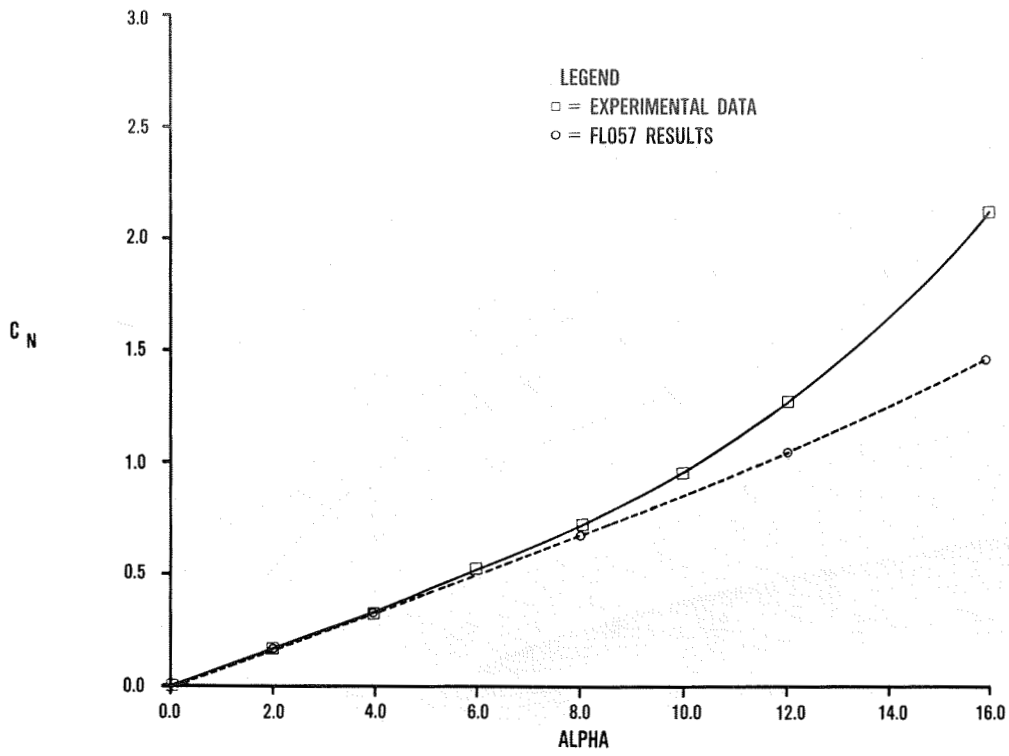
Figure 5.- Comparison of Euler and Ref. 1, C_N versus α.
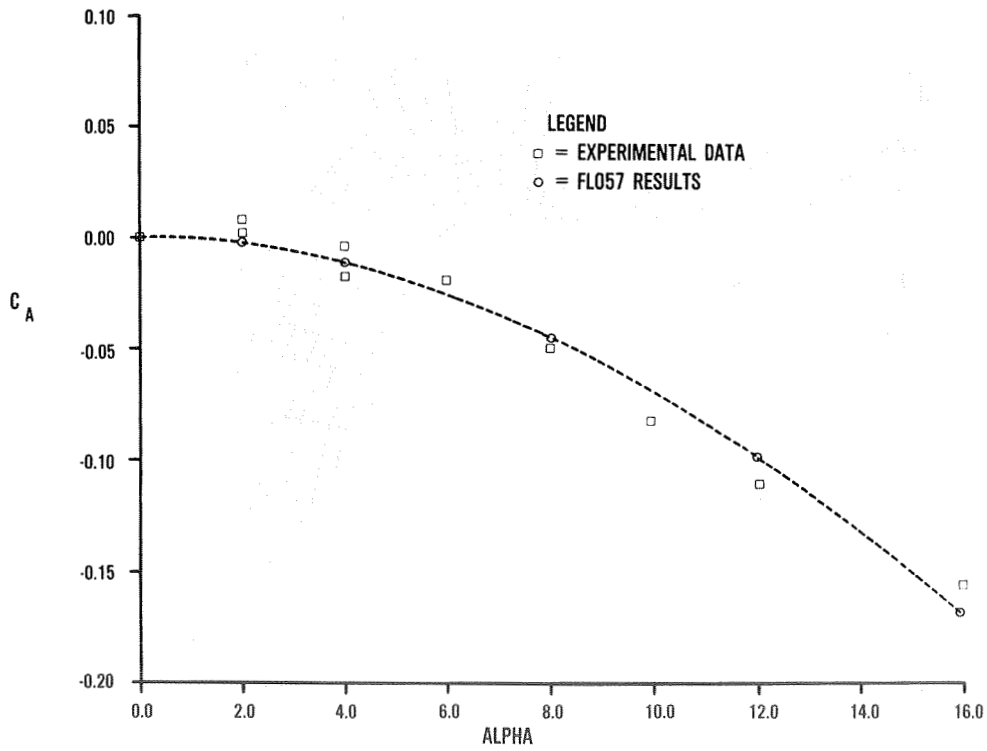
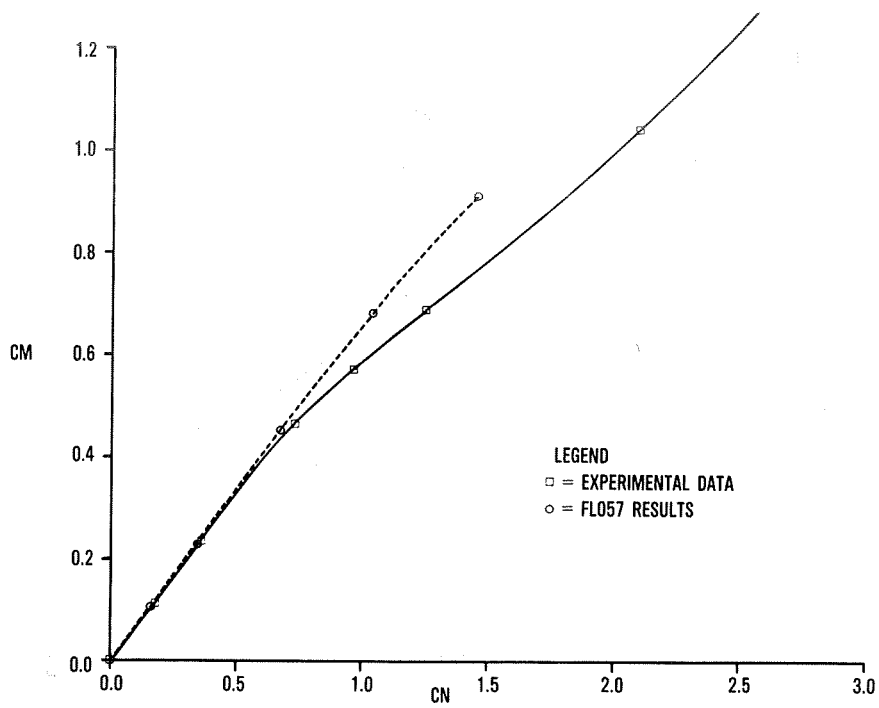Figure 6.- Comparison of Euler and Ref. 1, C_A versus α.

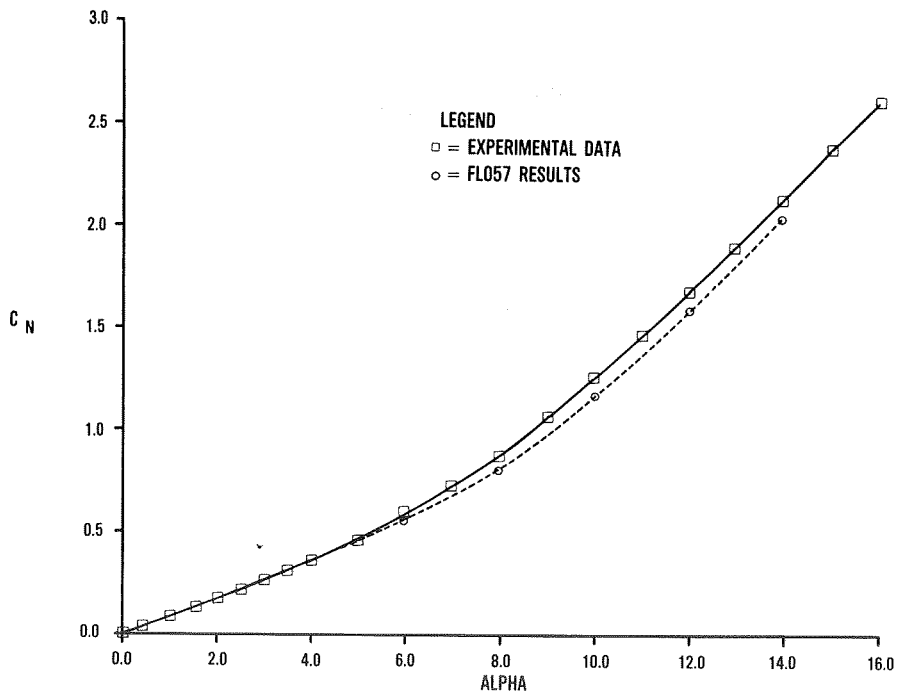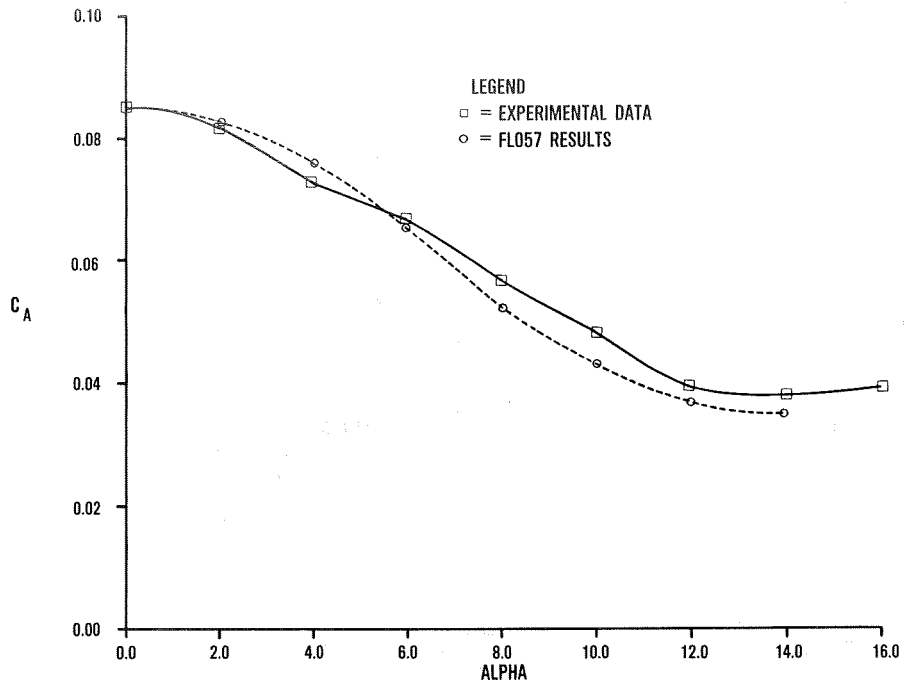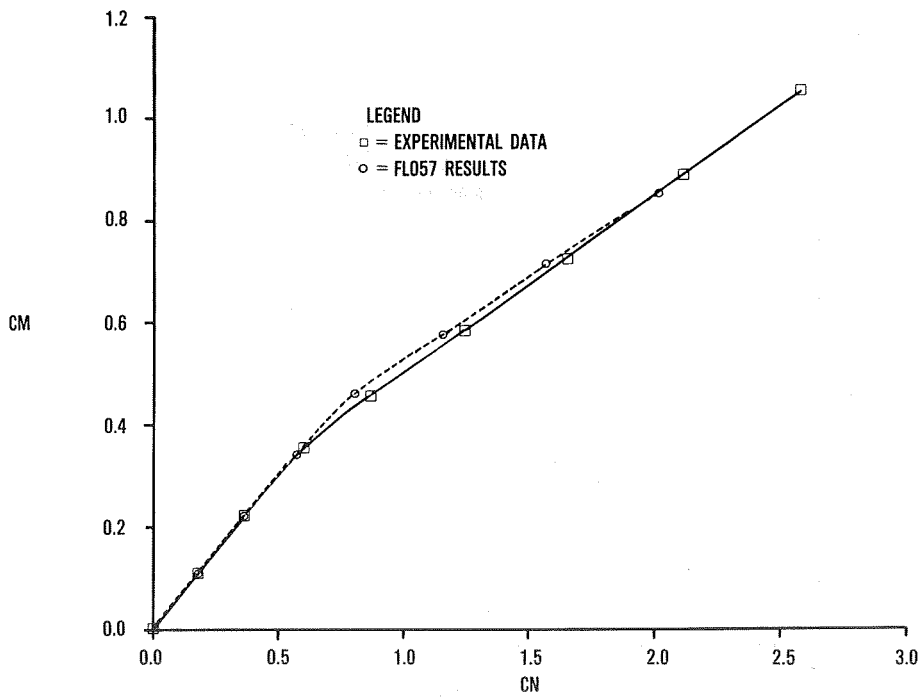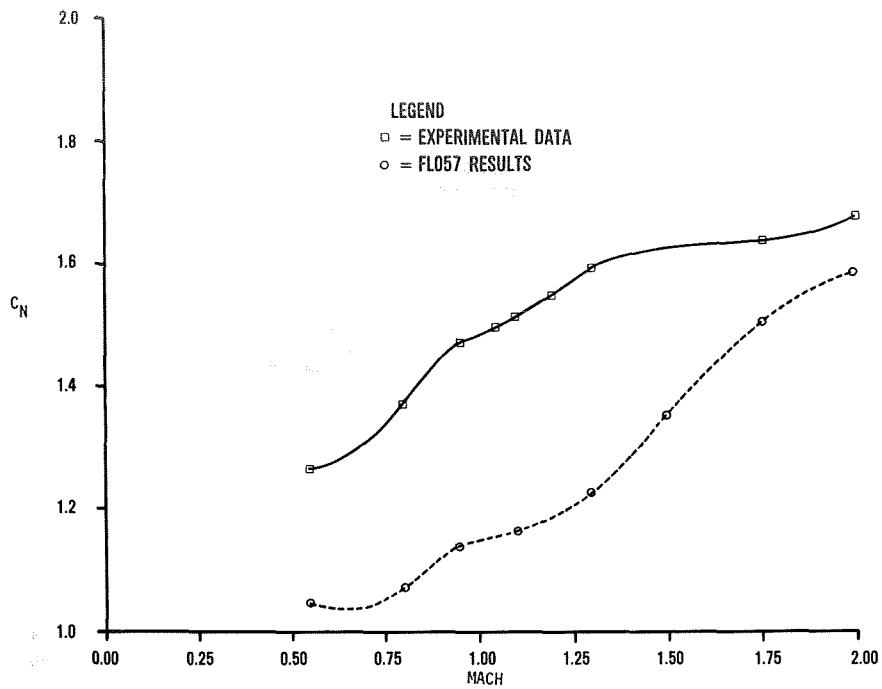Figure 7.- Comparison of Euler and Ref. 1, C_M versus C_N.

Figure 8.- Comparison of Euler and Ref. 1, C_N versus α.

Figure 9.- Comparison of Euler and Ref. 1, C_A versus α.

Figure 10.- Comparison of Euler and Ref. 1, C_n versus C_N.

Figure 11.- Comparison of Euler and Ref. 1, C_N versus Mach,
AL = 12.0 degrees.
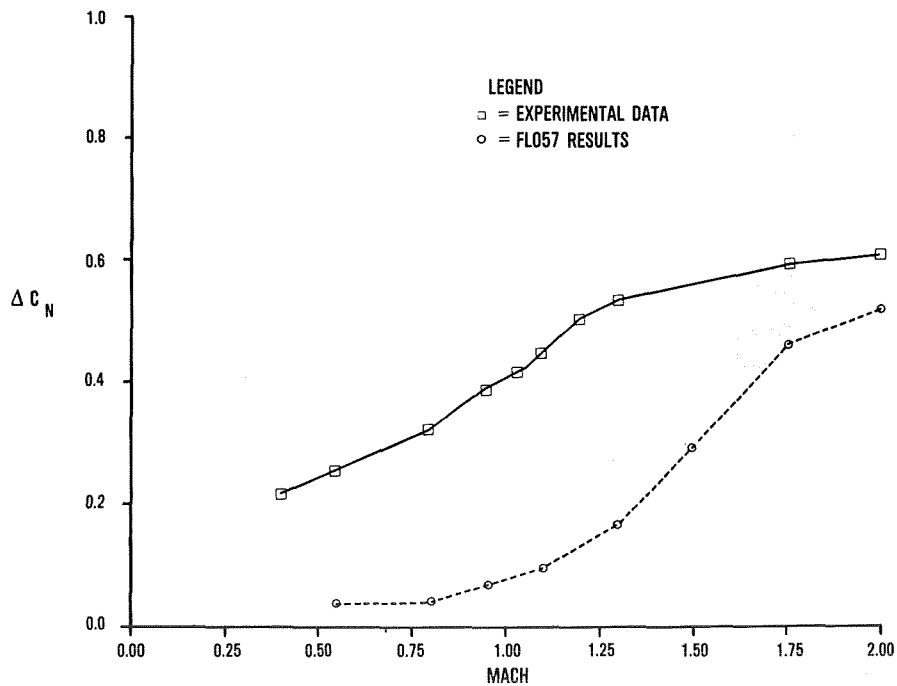
Figure 12.- Comparison of Euler and Ref. 1, ΔC_N versus Mach,
AL = 12.0 degrees.
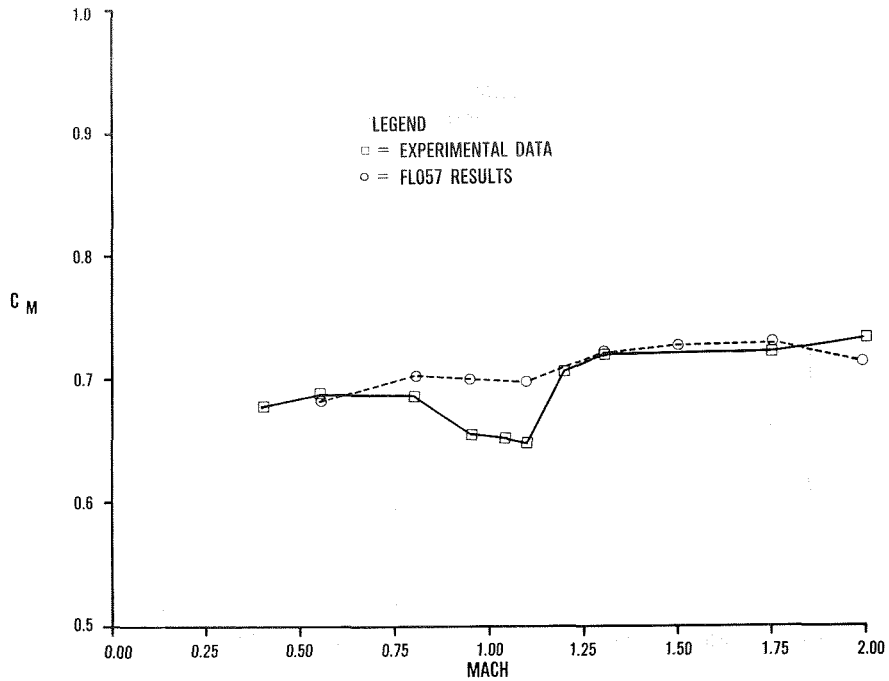
Figure 13.- Comparison of Euler and Ref. 1, C_M versus Mach,
AL = 12.0 degrees.

X STATION = 3.20
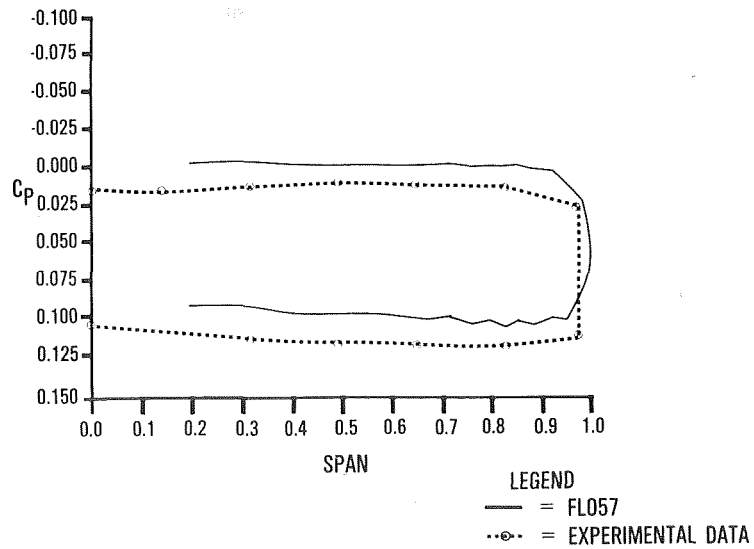
Figure 14.- Comparison of Euler and Ref. 1, C_p data,
M_∞ = 2.0, AL = 4.0, X = 3.20.

X STATION = 16.0
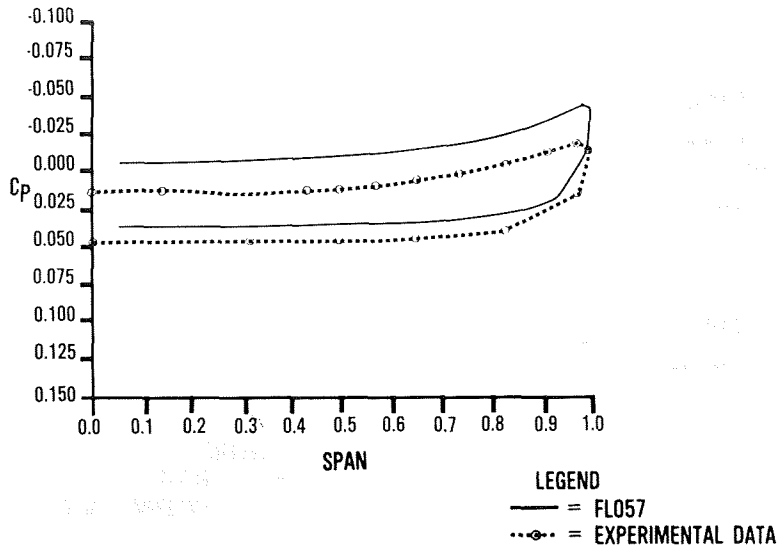
Figure 15.- Comparison of Euler and Ref. 1, C_p data,
M_∞ = 2.0, AL = 4.0, X = 16.0.

X STATION = 25.6
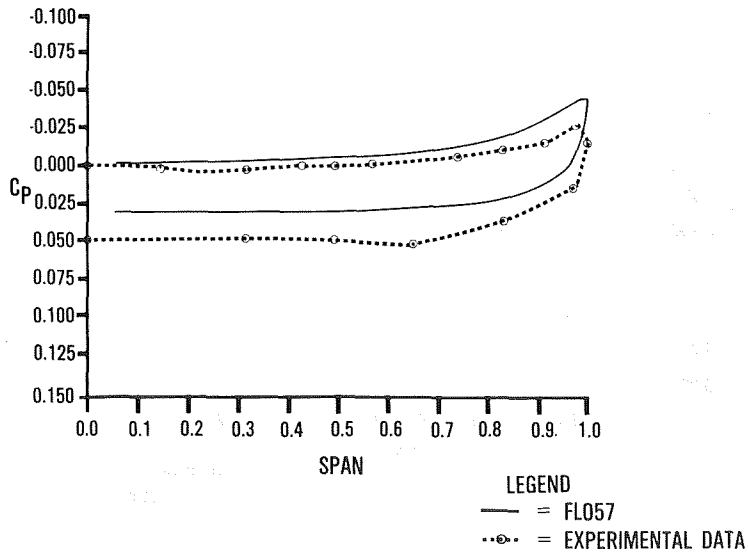
Figure 16.- Comparison of Euler and Ref. 1, C_p data,
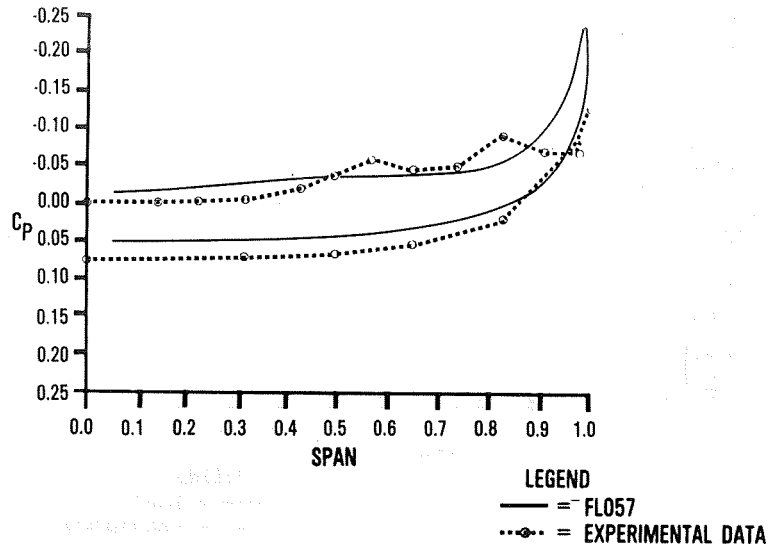M_∞ = 2.0, AL = 4.0, X = 25.6.

X STATION = 35.2
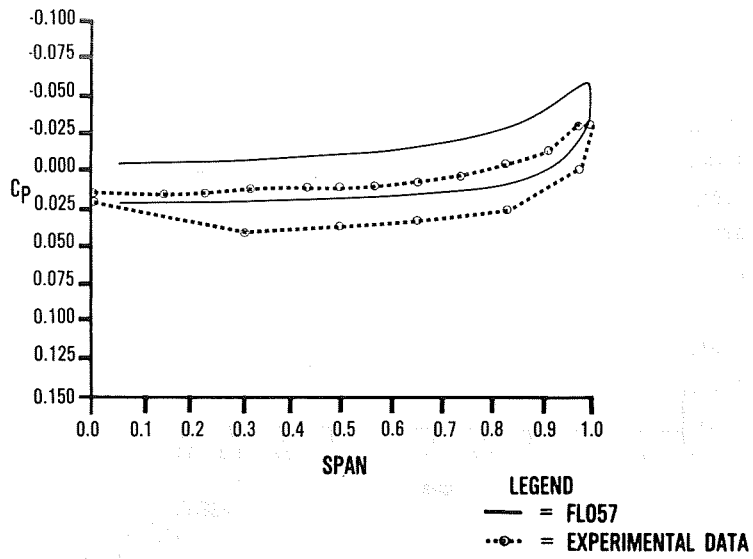
Figure 17.- Comparison of Euler and Ref. 1, C_p data, $M_\infty = 2.0$, AL = 4.0, X = 35.2.
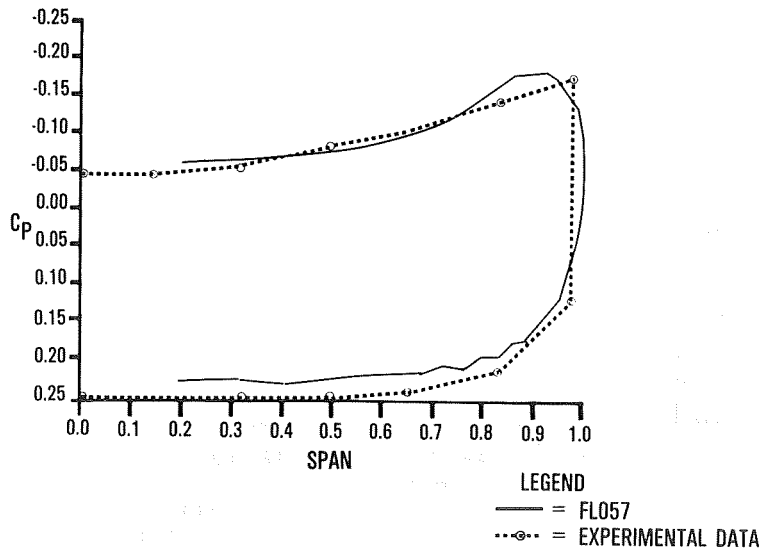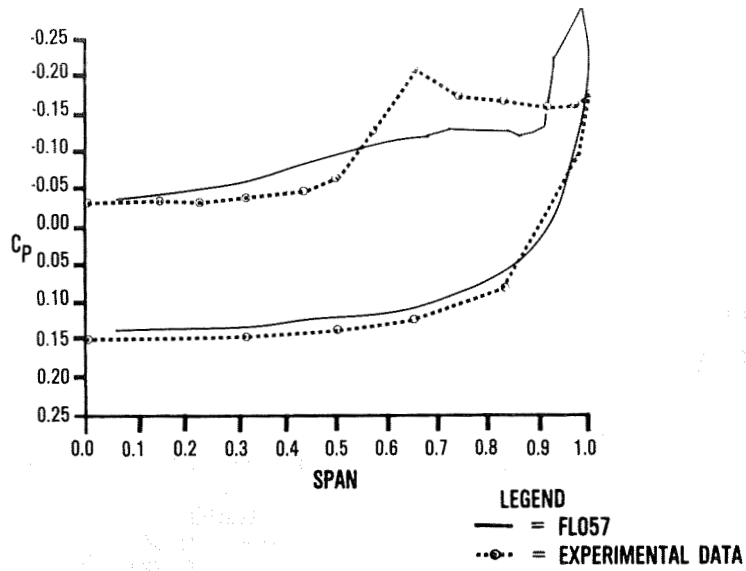
X STATION = 3.20
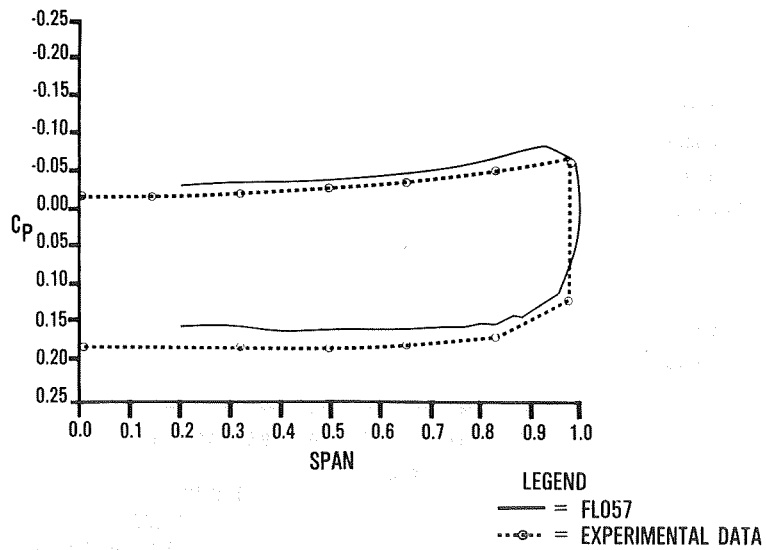
Figure 18.- Comparison of Euler and Ref. 1, C_p data, $M_\infty = 2.0$, AL = 8.0, X = 3.20.

X STATION = 16.0
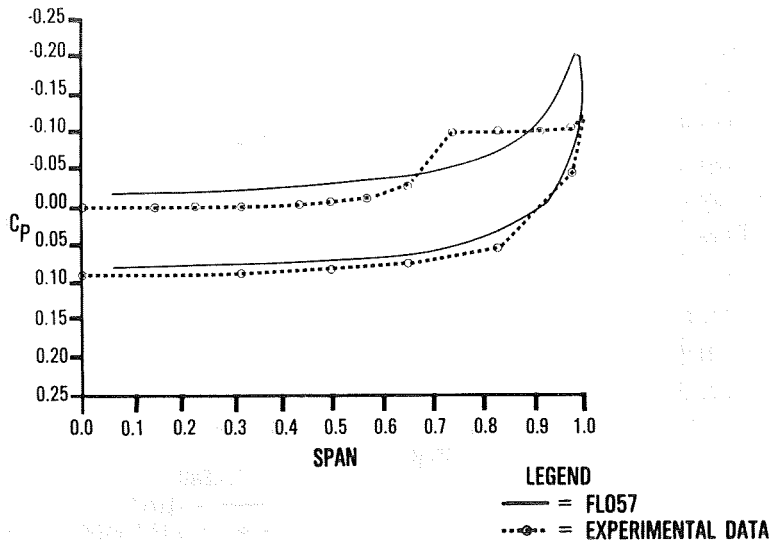
Figure 19.- Comparison of Euler and Ref. 1, C_p data,
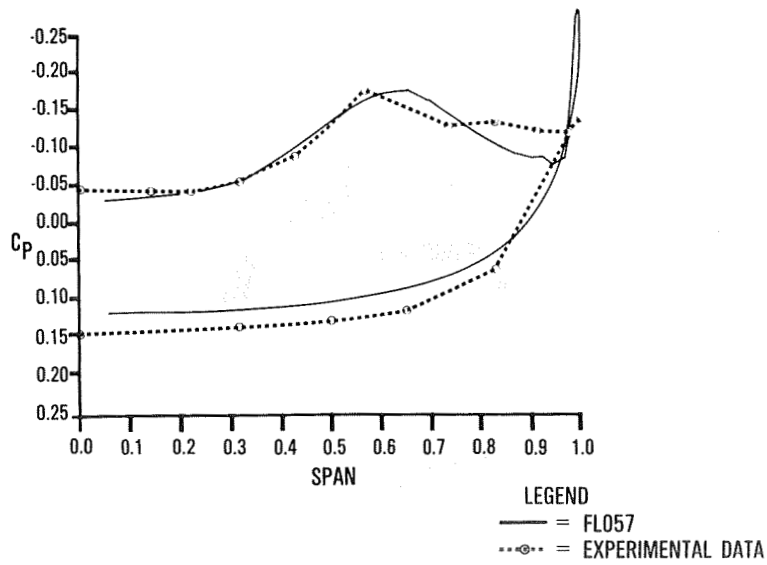M_∞ = 2.0, AL = 8.0, X = 16.0.

X STATION = 25.6
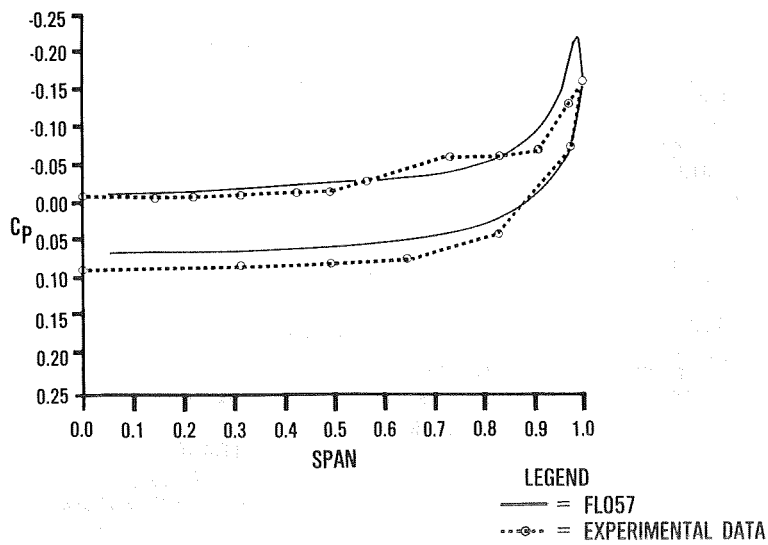
Figure 20.- Comparison of Euler and Ref. 1, C_p data,
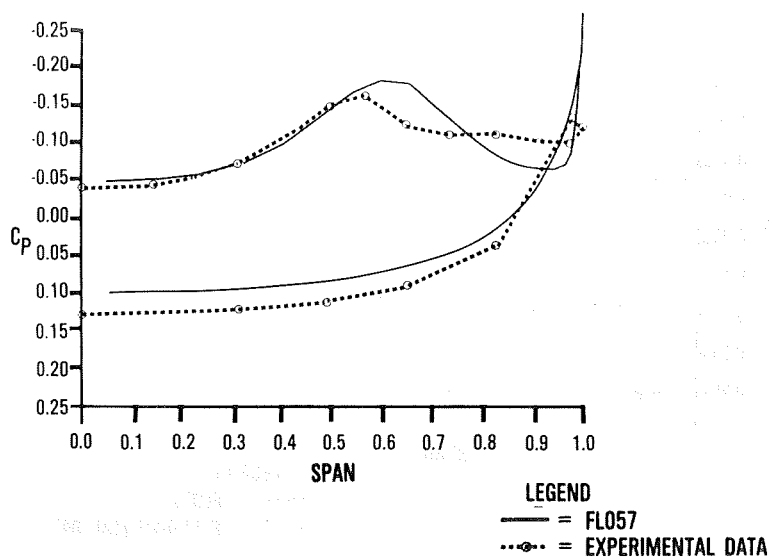M_∞ = 2.0, AL = 8.0, X = 25.6.

X STATION = 35.2

Figure 21.- Comparison of Euler and Ref. 1, C_p data,
$M_\infty = 2.0$, AL = 8.0, X = 35.2.

X STATION = 3.20

Figure 22.- Comparison of Euler and Ref. 1, C_p data,
$M_\infty = 2.0$, AL = 12.0, X = 3.20.

X STATION = 16.0

Figure 23.- Comparison of Euler and Ref. 1, C_p data, $M_\infty = 2.0$, AL = 12.0, X = 16.0.

X STATION = 25.6

Figure 24.- Comparison of Euler and Ref. 1, C_p data, $M_\infty = 2.0$, AL = 12.0, X = 25.6.

X STATION = 35.2

Figure 25.- Comparison of Euler and Ref. 1, C_p data,
M_∞ = 2.0, AL = 12.0, X = 35.2

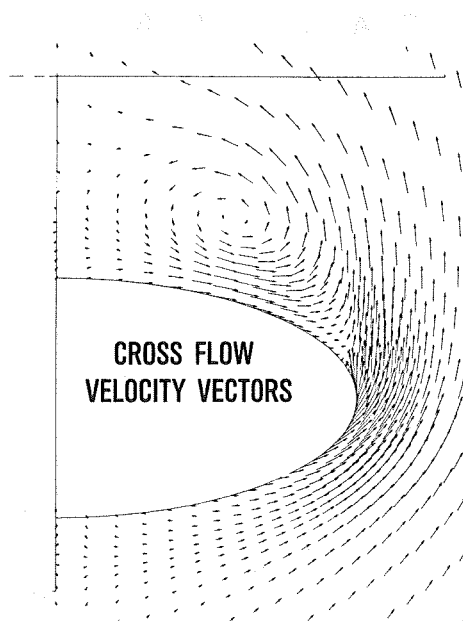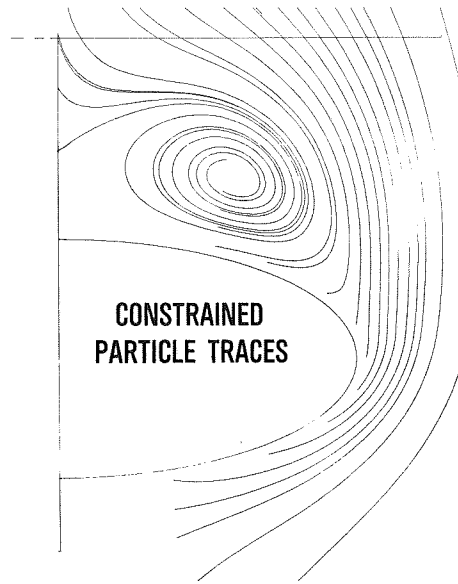Figure 26.- Cross-flow velocities,
M_∞ = 2.0, AL = 12.0, X = 35.2.

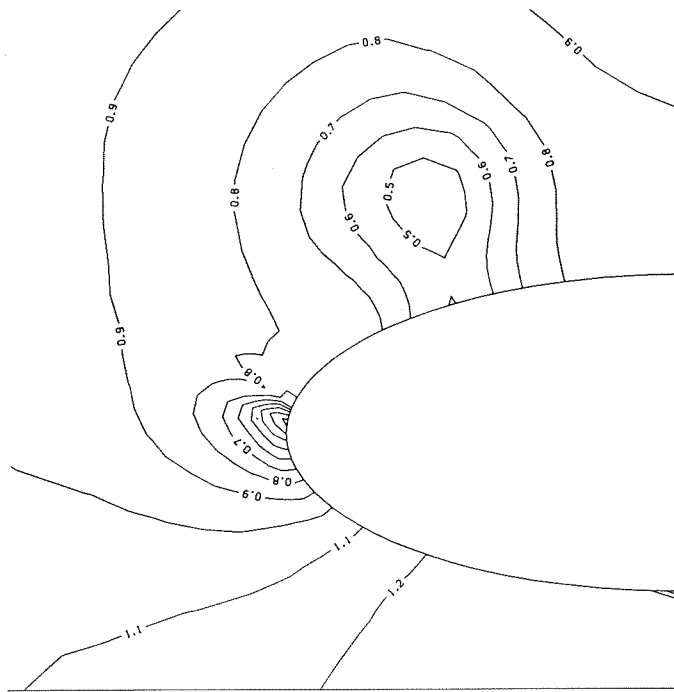Figure 27.- Constrained particle paths,
M_∞ = 2.0, AL = 12.0, X = 35.2.

Figure 28.- Static pressure contour plot, M_∞ = 2.0,
AL = 12.0, X = 35.2.

303